Available online at www.sciencedirect.com

SciVerse ScienceDirect

Journal of Terramechanics 50 (2013) 165–174

Journal of Terramechanics

www.elsevier.com/locate/jterra

Estimating terrain parameters for a rigid wheeled rover using neural networks

Matthew Cross *, Alex Ellery, Ala' Qadi

Department of Mechanical and Aerospace Engineering, Carleton University, 1125 Colonel By Drive, Ottawa, Canada K1S 5B6

Received 25 July 2012; received in revised form 4 April 2013; accepted 6 April 2013

Abstract

This paper presents a method for extracting data on regolith online with a planetary exploration micro-rover. The method uses a trained neural network to map engineering data from an instrumented chassis to estimates of regolith parameters. The target application for this method is a low-cost micro-rover scout on Mars that will autonomously traverse the surface and detect changes in the regolith cohesion and shearing resistance without the need for dedicated visual sinkage estimation on each wheel. This method has been applied to *Kapvik*, a low-cost 30 kg micro-rover analogue designed and built for the Canadian Space Agency. Data was collected using a motor controller interface designed for *Kapvik* using off-the-shelf components. The neural network was trained from parameters derived by classical terramechanics theory using Matlab's Neural Network Toolbox. The results demonstrate a proof of concept that neural networks can estimate the terrain parameters which may have applications for automated online traction control.

Keywords: Terrain parameter estimation; Neural network; Planetary rovers; Traction control

1. Introduction

The Mars Exploration Rover (MER) *Spirit* landed on the plains of Gusev Crater on 4 January 2004. Its original mission life was 90 Martian solar days, otherwise known as sols. *Spirit* continued to operate until sol 2210 when communication with Earth ended. Its right front wheel drive actuator failed during its extended mission. This failure caused the front right wheel to be pushed through the terrain instead of being driven. *Spirit* continued its extended exploration mission with five active wheels until it became embedded in loose terrain on sol 1871. Several attempts were made to extract *Spirit* from the loose soil. However, on sol 2104 the right rear wheel also failed which furthered impeded *Spirit*'s mobility. With only four functioning wheels, *Spirit* was unable to overcome the terrain resistance and continued to function merely as a stationary research base [1]. *Spirit* was not the only MER to be impeded by loose terrain. *Opportunity* encountered 30 cm of loose aeolian deposits at Meridiani Plains in which all six wheels became embedded. The rover required 23 Sols and 150 m of commanded wheel movements to move 26 cm and free itself from the "Purgatory Ripple" [2].

Spirit and *Opportunity* became immobilized due to the presence of a non-geometric obstacle: loose terrain. The loose terrain that trapped *Spirit* was believed to be a weakly cohesive mixture of sulfate and basaltic sands that caused the rover to experience greater wheel slip and wheel sinkage. The tractive force generated by the wheel-terrain interaction was not enough to overcome the terrain resistance. Classical terramechanics theory, with previously estimated terrain parameters, validated this conclusion [1].

The purpose of this work is to provide a proof of concept of estimating two Mars terrain parameters, cohesion and shearing resistance, online during a micro-rover's traverse phase using trained neural networks. Mars soil is herein referred to as regolith. Micro-rovers are intended to be low-cost scouts for a larger class of rover, such as *Curiosity*

* Corresponding author. Tel.: +1 6132772291.
E-mail addresses: matthewcross@cmail.carleton.ca (M. Cross), aellery@mae.carleton.ca (A. Ellery), alaqadi@mae.carleton.ca (A. Qadi).

0022-4898/$36.00
http://dx.doi.org/10.1016/j.jterra.2013.04.002

Nomenclature

CAN	Controller Area Network
MER	Mars Exploration Rover
MLP	Multilayer Perceptron
MSE	Mean Square Error
RSD	Relative Standard Deviation
SEEG	Space Exploration Engineering Group

and *ExoMars*. The research includes the development of motor controller interface software that provides the inputs to the neural network. The research presented is an extension of the motor controller interface software developed for the *Kapvik* micro-rover.

1.1. Kapvik micro-rover

Kapvik, as shown in Fig. 1, is a 30 kg micro-rover analogue designed as a tool for further developing Canada's planetary exploration capabilities. The Space Exploration Engineering Group (SEEG) at Carleton University was responsible for the development of the mobility system. *Kapvik* has an instrumented six-wheeled rocker-bogie system with differential drive similar to NASA's fleet of exploration rovers: *Sojourner* [3], *Spirit* [2] and *Opportunity* [1], and *Curiosity* [4]. The rocker-bogie allows all six wheels to maintain ground contact to enhance mobility while allowing the rover to climb over rocks [5,6]. *Kapvik* was designed with a view to flight qualification, and to help assess potential exploration missions to which Canada may contribute. It was designed for temperatures associated with summer in the high arctic. Its trial operations will be in an unknown environment-likely in the Canadian Arctic-analogous to the Mars equatorial surface.

Fig. 1. *Kapvik*'s mobility system, including the motor controller interface, was developed by the SEEG team at Carleton University.

1.2. Related works

Classical terramechanics theory developed by Bekker [7] and later Wong [8] has been applied to planetary vehicles since the Apollo program [9,10]. Much of the recent research on applying terramechanics to planetary rovers has been led by the Massachusetts Institute for Technology (MIT) Field and Space Robotics Laboratory and MIT Robotic Mobility Group. Therefore, the simplified wheel-terrain interaction model in this paper is based upon their research [11–13]. Many other research groups have been researching terramechanics for planetary rovers. The Space Robotics Laboratory at Tohoku University has been developing autonomous traction control for planetary rovers [14,15]. The terramechanics of wheel grousers for planetary rovers has been researched at Dalhousie University [16,17]. Current planetary rover research in Europe is studying flexible wheels [18,19].

Online terrain classification and estimation has also been studied. Kleiner [20] successfully classified terrain based on vision and wheel vibrations; however, the terrain greatly varied (grass versus asphalt versus gravel) and there was no indication this classification method could detect changes in the properties of a single terrain type. Brooks [21,22] also used wheel vibrations to classify between more similar terrain types but not to estimate terrain parameters. Tan [23] and Yousefi Moghaddam [24] each proposed a method for estimating terrain parameters online; however their application was for excavation and not based on wheel-terrain interaction. Iagnemma used a simplified wheel-terrain interaction model [11–13] for estimating the two terrain parameters online for an exploration rover. He solved for $[c, \phi]$ using linear least squares with a set of sensor data $[V, \omega, z, I]$, a quasi-static wheel load W, and assumed shear deformation parameter K. His laboratory experiments, using an instrumented testbed, showed that the least squares estimates for $[c, \phi]$ of the sand were within range of the bevameter measurements. An *a priori* value for the shear deformation parameter K was needed to solve the least squares estimate. He also estimated the terrain parameters for a six-wheeled rover in a Matlab

simulation using simulated noisy sensor data. His simulation results showed that the least squares estimates of sand were within error. Iagnemma's simulation did not describe how the wheel sinkage z, or wheel-terrain contact area A, was measured; only a simulated value was used for the estimation of the terrain parameters.

The wheel sinkage z estimates are used to calculate the wheel-terrain contact arc $\theta_C = \cos^{-1}(1 - z/r)$. Wilcox [25] estimated z on a six-wheeled articulated rover similar to *Sojourner* and *Kapvik*. His kinematic model worked well to detect sinkage but he noted the sensor noise was too high to give a good z estimate. Reina [26] used visual sinkage estimation to measure z however the size, mass, and power consumption required to support dedicated vision measurements of each wheel do not fit into the scope of a low-cost micro-class rover.

1.3. Outline

This paper continues with a description of the terrain parameter estimation method including the simplified wheel-terrain model. A brief introduction to neural networking is provided along with the procedure to construct the neural network used for this research. The neural network training set is then derived using the simplified wheel-terrain model. The results from field testing are provided followed by conclusions.

2. Terrain parameter estimation method

Iagnemma's simplified wheel-terrain interaction model [11–13] allows the terrain parameters to be a multivariable function of the sensor measurements $[c, \phi] = f(V, \omega, z, W, I)$:

- The rover velocity V is provided by a velocimeter;
- The motor rotational speed ω is provided by encoder data;
- The current drawn by the motor I is provided by the motor controller;
- The weight-on-wheels W is provided from load cells on each wheel; and
- The wheel sinkage z is unknown and is needed for the contact arc θ_C.

2.1. Simplified wheel-terrain interaction model

The terrain parameters $[c, \phi]$ are related to the wheel-terrain interaction model by the shear stress distribution equation along the wheel-terrain interface [8] (see Fig. 2):

$$\tau_m = (c + \sigma_m \tan\phi)\left(1 - e^{\frac{-j}{K}}\right) \quad (1)$$

where

- The shear deformation parameter K is experimentally derived for a particular terrain;

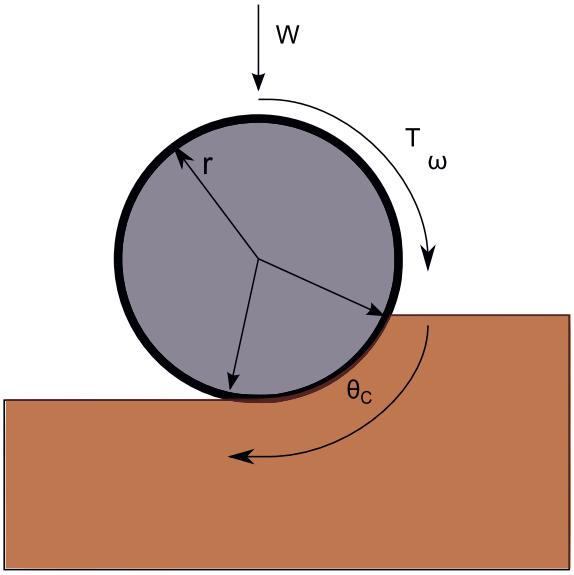

Fig. 2. Simplified wheel-terrain interface diagram. W is the weight on the wheels; T is the torque driving the wheel as determined by the motor current draw; ω is the rotational speed of the wheel as determined by the encoder; and θ_C is the wheel-terrain contact arc.

- c is the terrain cohesion and one of the parameters to be estimated;
- ϕ is angle of shearing resistance and is the other parameter to be estimated;
- The amount of slippage $j = f(i, \theta_C)$ is determined by the slip ratio $i = 1 - V/r\,\omega$ from the rover velocity V and the motor shaft rotational speed ω;
- The maximum shear stress $\tau_m = f(I, \theta_C)$ over the wheel contact area $A = rw\theta_C$ is determined from the torque T applied by the motor, which draws a current I;
- The maximum normal stress $\sigma_m = f(W, \theta_C)$ is determined by the wheel load W acting over A; and
- The wheel radius r and width w are known values.

The shear stress τ_m acting over A determines the maximum allowable thrust $F = f(\tau_m)$. Therefore, $[c, \phi]$ influence the mobility of a rigid-wheeled vehicle on terrestrial and planetary terrain. A decrease in either c or ϕ will result in a decrease in the maximum thrust available at the wheel. When the thrust available is less than the resisting force of the terrain, the wheel becomes immobilized. The force and torque balance of the wheel-terrain interface is given in Eqs. (2) and (3):

$$W = rw\left(\int_{\theta_2}^{\theta_1} \sigma(\theta)\cos\theta\,\mathrm{d}\theta + \int_{\theta_2}^{\theta_1} \tau(\theta)\sin\theta\,\mathrm{d}\theta\right) \quad (2)$$

$$T = r^2 w \int_{\theta_2}^{\theta_1} \tau(\theta)\,\mathrm{d}\theta \quad (3)$$

The normal stress $\sigma(\theta)$ is divided into two regions on either side of the maximum normal stress σ_m, where θ is an angle relative to vertical axis. The normal stress in

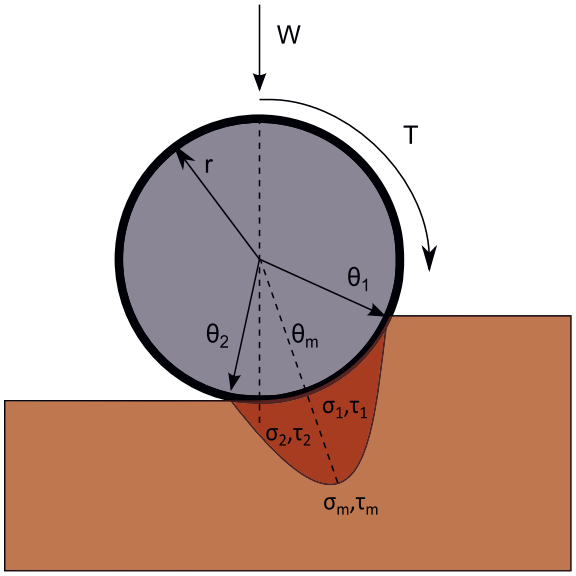

Fig. 3. Simplified wheel-terrain interface diagram showing normal σ and shear stress τ distribution.

Region 1, σ_1, occurs in the region between the wheel-terrain interface entry point θ_1 and the maximum stress point θ_m; The normal stress in Region 2, σ_2, occurs in the region between θ_m and the interface exit point θ_2. These regions of normal stress are shown in Fig. 3. Iagnemma [12,13] states that σ_m and τ_m can be assumed to be co-located at the same angle θ_m "for a wide range of soil values". With these linearization assumptions, the simplified stress distribution along the wheel-terrain interface can be shown:

$$\sigma(\theta) = \begin{cases} \sigma_1(\theta) = \frac{\theta_1-\theta}{\theta_1-\theta_m}\sigma_m & \text{for } \theta = \theta_1 \rightarrow \theta_m \\ \sigma_2(\theta) = \frac{\theta-\theta_2}{\theta_m-\theta_2}\sigma_m & \text{for } \theta = \theta_m \rightarrow \theta_2 \end{cases} \quad (4)$$

$$\tau(\theta) = \begin{cases} \tau_1(\theta) = \frac{\theta_1-\theta}{\theta_1-\theta_m}\tau_m & \text{for } \theta = \theta_1 \rightarrow \theta_m \\ \tau_2(\theta) = c + \frac{\theta-\theta_2}{\theta_m-\theta_2}(\tau_m - c) & \text{for } \theta = \theta_m \rightarrow \theta_2 \end{cases} \quad (5)$$

Iagnemma further states that the maximum stresses occur approximately midway along the contact angle $\theta_m = \frac{1}{2}(\theta_1 + \theta_2)$, and this is "reasonable for a wide range of soils". The exit angle θ_2 is taken to be approximately 0 (in line with the vertical axis) [12,13]. The wheel-terrain contact arc spans the angle between the entrance angle and the exit angle, $\theta_C = |\theta_1 - \theta_2|$. With these simplifying assumptions Eq. (2) reduces to Eqs. (6) and (3) reduces to Eq. (7):

$$W = \frac{rw}{\theta_C}\left(c\theta_C - 2\sigma_m(1+\cos(\theta_C) - 2\cos(\frac{\theta_C}{2})) - 2\tau_m(\sin(\theta_C) - 2\sin\left(\frac{\theta_C}{2}\right)) - 2c\sin\left(\frac{\theta_C}{2}\right)\right) \quad (6)$$

$$T = \frac{1}{2}\left(\tau_m + \frac{c}{2}\right)r^2 w\theta_C \quad (7)$$

The final unknown variable z is needed to estimate $[c, \phi]$ using classical terramechanics theory. The mapping $[c, \phi] = f(V, \omega, z, W, I)$ exists as an approximate function even if z is unknown. Trained neural networks have been shown to be universal function approximators [27]; here we use them to map the terrain parameters $[c, \tan\phi]$ as a function of the sensor values $[W, i, I]$.

2.2. Neural network

We have established the simplified wheel-terrain interaction model in the previous section to show the terrain parameters to be a function of the sensor values. We will then use a neural network to approximate that function. This section gives a brief introduction to the concepts of neural networks.

Neural networks contain a set of artificial neurons. An artificial neuron q has four components:

- The vector input signal, $\mathbf{x} \in \Re^{n\times 1}$ is multiplied by the synaptic weights, $\mathbf{w_q} \in \Re^{n\times 1}$;
- A bias or threshold x_0 is connected to the summing junction by a synaptic weight w_{q0} and acts to raise or lower activity level of the neuron;
- The output of the summation junction, v_q, is then passed through an activation function, $f(\cdot)$. For the application described in this paper, the activation function is a binary sigmoid function $f_{bs}(v_q) = \frac{1}{1+e^{-v_q}}$ with saturation levels at 0 and 1; and
- The output of the activation function $u_q = f\left(\sum_{j=0}^{n} w_{qj}x_j\right)$ is the axon.

When the axon u_q is the output of the neuron is denoted as y_q [28,29].

There is a wide range of neural network types that are used for different applications. A static feed forward multilayer perceptron (MLP) is used for the application described in this paper. A MLP contains more than one layer of artificial neurons.

- The "zero" layer is the vector input signal, which contain the sensor values $\mathbf{x} \in \Re^{n\times 1} = [W, i, I]$;
- $\mathbf{x} \in \Re^{n\times 1} = [W, i, I]$feeds into the first "hidden" layer of neurons. There may be more than one hidden layer depending on the network architecture. One layer of a large enough number of hidden neurons is sufficient for function approximation [27]. For the MLP described in this paper, only one layer is used.

- The last hidden layer fires synapses into the output layer that provides the vector response signal, which contain the terrain parameter estimates $\mathbf{y} \in \Re^{m\times 1} = [c, \tan\phi]$.

The MLP is trained with backpropagation [28–30] to approximate a desired signal or pattern. Backpropagation is a gradient descent method for updating the weights of a MLP during training. The training goal is to minimize the mean square error (MSE) between network output $\mathbf{y} \in \Re^{m\times 1} = [c, \tan\phi]$ and the desired output $\mathbf{d} \in \Re^{m\times 1} = [c, \tan\phi]$. The weights of output layer S are

updated based on the error $e = d - y$, the learning rate μ, and the output of the layer u: $\Delta w_{ji}^S = \mu^S \delta_j^S u^{S-1}$ where the local delta error is $\delta_j^S = ef'\left(v_j^S\right) = eg(v_j^S)$ and f' is the derivative of the activation function. The learning rate is a variable parameter in Matlab that gets automatically re-evaluated after each epoch. The weights on the hidden layer are updated in a similar manner.

2.3. Network sizing

The number of neurons in the hidden layer is based upon the size of the training set. Georgio [31] and Bartlett [32] each provide different formulations to size the hidden layer. Here we use both neuron sizes as the range for statistical analysis. The range of optimal hidden neurons is determined from Georgio's equations [31], and Bartlett's linear relation (each neuron has six connections: 3 input, 2 output and 1 bias) [32]. The MLP was trained 100 times for each number of hidden neurons in the range. The number of hidden neurons that resulted in the best mean MLP performance (lowest mean mean-square-error (MSE)) was set as the optimal hidden layer size. Matlab Neural Network Toolbox is used for the MLP performance testing. The training goal was set to be an MSE of 0.005, or 10,000 epochs, whichever came first. Several runs showed the network would converge after approximately 5000 epochs, and runs for 100,000 epochs showed no further improvement. The steps to get the optimal number of hidden neurons are as follows:

Step 1: Get size of training set.
Step 2: Get range of hidden neurons for statistical network training.
Step 3: Run the MLP 100 times to determine the mean MSE.
Step 4: Repeat Step 3 over the range of neurons.
Step 5: The hidden neuron number that results in the lowest MSE is selected as the optimal size.

2.4. Offline MLP construction

This section outlines the method of constructing the MLP to estimate terrain parameters. The MLP is first designed (Steps 1–3) and trained (Steps 4–6) offline before it is used for parameter estimation. Training set construction is described in detail in Section 3.1.

Step 1 Define the number of neurons in the hidden layer.
Step 2 Initialize the synaptic weights with Nguyen-Widrow algorithm [33].
Step 3 Define a MSE to be used as the training goal.
Step 4 Present input pattern from training set and compare the MLP output to the desired output:

- The vector input signal, $\mathbf{x} \in \Re^{n\times 1} = [W, i, I]$ feeds into the hidden layer.
- For each hidden neuron:
  - $\mathbf{x} \in \Re^{n\times 1} = [W, i, I]$is multiplied by the synaptic weights, $\mathbf{w_q} \in \Re^{n\times 1}$.
  - The $x_0 = 1$ bias is multiplied by its respective synaptic weight w_{q0}.
  - The output of the summation junction, v_q, is then passed through an activation function, $g_{bs}(v_q) = \frac{1}{1+e^{-xv_q}}$.
  - The output of the activation function, u_q is the axon.
- The hidden layer fires synapses into the output layer which provides the vector response signal, $\mathbf{y} \in \Re^{m\times 1} = [c, \tan\phi]$.
- The network output $\mathbf{y} \in \Re^{m\times 1} = [c, \tan\phi]$is compared to the desired output $\mathbf{d} \in \Re^{m\times 1} = [c, \tan\phi]$.
- The error between the desired output and the MLP output $\mathbf{e} = \mathbf{d} - \mathbf{y}$ becomes the basis for weight adjustments.

Step 5 Adjust weights with backpropagation until the defined training goal is met.
Step 6 The MLP is 'frozen' and ready to be used for estimating parameters.

It should be noted that the MLP output is $[c, \tan\phi]$ and is post-processed to give an angular value of ϕ. The MLP in operation will take the input vector $[W, i, I]$ and map it to an output vector $[c, \tan\phi]$ as per its training.

3. Verification experiment

A MLP was constructed to map the sensor values taken during *Kapvik*'s field testing $[W, i, I]$ to the terrain parameters $[c, \tan\phi]$. The MLP must first be trained using a set of input–output pairs before it can be used for parameter estimation. This section describes the process by which the MLP was trained, and tested using data collected from the *Kapvik* rover.

3.1. MLP set construction

This section describes how the sets of training pairs were constructed in Matlab using the simplified wheel-terrain interaction model. Each training pair consists of inputs (wheel-terrain interface variables $[W, i, I]$) and outputs (terrain parameters $[c, \tan\phi]$). The set of terrain parameters are taken from terrestrial soil classes in Table 1. The interface variables $[z, i, I]$ are defined as representative values observed during testing; the range of motor currents ($I = 50, 60, 70, 80, 90, 100$ mA), wheel slip ($i = 0.01, 0.02, 0.03$), and wheel sinkage values ($z = 0.005, 0.0075, 0.01, 0.0125, 0.015, 0.0175, 0.02$ m). The objective is to determine, for a given terrain and wheel interaction, the sensor values expected to be observed as determined by the simplified model. This procedure creates a set of training pairs that map $[W, i, I]$ to $[c, \tan\phi]$ and is given as follows:

Step 1: Define wheel dimensions r and w.
Step 2: Get $[c, \phi, K]$ set from one terrain class.

Step 3: Get $[z]$ and $[i]$ from the defined sets to calculate the sinkage due to shear loading, also known as slip sinkage, z_{SS}, using Lyasko's analytic formulation [34]:

$$z_{SS} = \left(\frac{1+i}{1-0.5i}\right)z \tag{8}$$

Step 4: Calculate θ_C, taking slip sinkage into account, from z_{SS}, r, and w

$$\theta_C = \cos^{-1}\left(1 - \frac{z_{SS}}{r}\right) \tag{9}$$

Step 5: Use $[i]$ to calculate j

$$j = r\ (\theta_C + i\ \sin\ (\theta_C) - \sin\ (\theta_C)) \tag{10}$$

Step 6: Define the gearing ratios ζ and transmission efficiencies η of the harmonic drive (HD) and planetary gears (PG); define the motor torque constant κ; get $[I]$ to calculate T

$$T = \kappa\zeta_{PG}\zeta_{HD}\eta_{PG}\eta_{HD}I \tag{11}$$

Step 7: Calculate τ_m by rearranging Eq. (7)

$$\tau_m = \frac{2T}{wr^2\theta_C} - \frac{c}{2} \tag{12}$$

Step 8: Calculate σ_m by rearranging Eq. (1)

$$\sigma_m = (\tan\phi)^{-1}\left(\frac{\tau_m}{1-e^{-j/K}} - c\right) \tag{13}$$

Step 9: Calculate W with Eq. (6)

$$W = \frac{rw}{\theta_C}\left(c\theta_C - 2\sigma_m\left(1 + \cos(\theta_C) - 2\cos\left(\frac{\theta_C}{2}\right)\right) - 2\tau_m\left(\sin(\theta_C) - 2\sin\left(\frac{\theta_C}{2}\right)\right) - 2c\sin\left(\frac{\theta_C}{2}\right)\right) \tag{14}$$

Step 10: Create Input $[W, T, i]$ and Output $[c, \tan\phi]$ pair.
Step 11: Repeat Steps 6–10 for each I in the motor current training set.
Step 12: Repeat Steps 5–11 for each i in the wheel slip training set.
Step 13: Repeat Steps 3–12 for each z in the wheel sinkage training set.
Step 14: Repeat Steps 2–13 for each terrain class.
Step 15: Randomize order of training pairs.

These variations resulted in 504 training pairs. Several training runs showed that randomizing the order of the training pairs improved the MLP's ability to converge. The neuron range for statistical analysis was from 59 to 84 neurons; 64 neurons were found to have the lowest mean MSE. The 3:64:2 MLP was trained by backpropagation with momentum and learning updating for 10,000 epochs and a MSE of 0.0251 was reached. The MLP was set to 3:64:2 for terrain parameter estimation.

Table 1
Terrestrial soil parameters used in MLP training.

Soil	c (kPa)	ϕ	K (m)
LETE sand	1.22	30.3°	0.0116
Sandy loam	3.15	30.0°	0.0420
Clayey soil	4.12	11.8°	0.0254
Medium soil	6.41	25.7°	0.0238

3.2. Kapvik field testing

Kapvik's mobility system, as shown in Fig. 4, was tested at Petrie Island, located in the east end of Ottawa along the Ottawa River, over two days in September 2011. Petrie Island is a municipal park that has a flat sandy section (approximately 100 m in length), which was found to be suitable for testing. The field testing was conducted according to the verification test plan to verify the mechanical performance of *Kapvik*'s instrumented mobility system. The test plan required *Kapvik* to be loaded to its design mass of 30 kg and traverse a variety of obstacles, distances, and terrain conditions. For each test condition, *Kapvik*'s designed speed was set to 2.2 cm/s. The motor controller interface software collected $[W, \omega, I]$ at 2 Hz.

Kapvik ran two additional tests at Petrie Island: one 10 m traverse over prepared terrain and one 10 m traverse over unprepared terrain. The prepared terrain consisted of sand that had been raked level. The unprepared terrain was as it was found: uneven with windswept footprints. The data from these additional tests was used for post-test analysis but not for on-line operation nor navigation purposes.

The mobility testing was performed before *Kapvik* was fully integrated, and before online terrain parameter estimation was considered. A speckle velocimeter [35] was not available to provide V needed to calculate i. The slip ratio was derived as follows: *Kapvik* was commanded to traverse 10 m as determined by ω; the motor control interface software calculates how long to leave the motors running at a constant speed (2.2 cm/s) for the wheels to have rotated the equivalent of 10 m (454.54 s); the final distance travelled was 9.75 m for an average i of 0.025. A constant slip ratio of 0.025 was appended to the I and W data sets consisting of 909 data points were recorded during the traverse.

3.3. Results and discussion

The 500th data set was arbitrarily selected from the 909 to test the trained MLP; from that set the current ($I = 80$ mA) and wheel load ($W = 31.6$ N) from the 5th wheel were selected. These two values, along with the averaged slip ratio of 0.025, were entered into the trained 3:64:2 MLP. The output of the network gives the estimate of cohesion to be 3352 N and the shearing angle to be 28.6°. Both of these results are consistent with reported values of sandy loam [8] as show in Table 2, which was to be expected.

It should be noted that the terrain parameters were not measured at the time of the mobility testing; the idea of

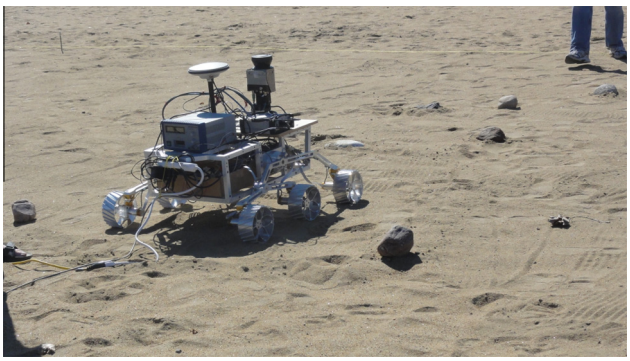

Fig. 4. *Kapvik*'s mobility system was tested at Petrie Island in Ottawa, Canada. Tests were performed at full load in sandy terrain. *Kapvik* successfully navigated all required obstacles.

Table 2
Reported parameters of various terrains, from Wong [8].

	c (kPa)	ϕ (°)
LETE sand	1.15	31.5
LETE sand	1.39	30.6
Sand	1.3	31.1
Sandy loam	3.3	33.7
Sandy loam	3.4	24.1
Sandy loam	4.3	22.7
Sandy loam	3.7	29.8
Sandy loam	3.2	30.5
Loam	3.45	30.1
Clayey soil	3.45	11.0
Clayey soil	7.58	14.0
Soft soil	3.71	25.6
Medium soil	6.89	29.0
Medium soil	8.62	22.5

estimating terrain parameters from the sensors values did not arise until after mobility testing and as such the true terrain parameters were not required at the time. As the *Kapvik* chassis was delivered shortly after the mobility tests, there was no available platform to collect data at the same time as taking bevameter measurements. Therefore, the estimated parameters were compared only to the reported values in Table 2. However, in his review of soil strength measurement techniques, Okello [36] highlights the variability of terrain parameter estimation by different techniques. The bevameter technique most closely simulates wheel-terrain interaction; however, measurements are static and do not account for slippage or slip-sinkage that dynamically occur in wheel-terrain interaction. Furthermore, Okello states that "there seems to be no standard, proven and above all, reliable technique currently available that can be universally applied to measure soil strength parameters appropriate to prediction of vehicle performance" [36].

Okello's statement suggests to us that directly measuring the terrain parameters using different techniques would not yield the same values each time or for each technique. However, we assume that measured values would be consistent within a range; measuring the terrain parameters at Petrie Island would produce a range of values depending on the measurement method. Therefore, we are not able give a definite range of error for our estimates using the MLP because there are no absolute values for comparison. For this reason, we deem reasonable comparisons to the reported values in Table 2 to be sufficient for the proof of concept.

The entire data set for all six wheels on prepared terrain was processed. The results for Wheel 3 (see Fig. 5 for wheel numbering) are shown in Figs. 6 and 7. Fig. 6 shows the cohesion to be mostly between 3200 and 4000 Pa with a mean of 3726 Pa and relative standard deviation (RSD) of 6.4%, which is to be expected from the terrain at Petrie Island. Fig. 7 shows the shearing resistance angle to be between 26° and 30° with a mean of 27.8° and RSD of 6.5%, which is consistent with sandy loam. Table 3 lists the estimates from all six wheels. The RSD for the estimates can be compared to the RSD of sensor data in Table 4.

The three largest deviations in shearing resistance angle correlate to the three spikes in cohesion. This is attributed to current data noise in which the reported current dropped momentarily. The drop in current translates to a drop in required torque to move the wheel which would be observed if the terrain had a higher cohesion. The MLP would report that to be more clayey loam-like based on the training set.

The data collected from the traverse over unprepared terrain was then inputted to the MLP. The results for Wheel 3 are shown in Figs. 8 and 9. Fig. 8 shows the cohesion to be mostly between 3200 and 4000 Pa with a mean of 3722 Pa and RSD of 6.7%, which is to be expected from the sand at Petrie Island. Fig. 9 shows the shearing resistance angle to be between 26° and 30° with a mean of 27.8° and RSD of 6.5%, which is consistent with sandy loam. Table 5 lists the estimates from all six wheels. The RSD for the estimates can be compared to the RSD of sensor data in Table 6.

These results show that there is little difference in the estimates between prepared and unprepared terrain. In both cases, all six wheels given similar results, as expected. The RSD is similar between the cohesion and shearing resistance angle estimates for each wheel.

Comparing the results (Table 3) to the sensor noise (Table 4) shows how higher sensor noise results in greater variance in the estimates. In both cases, wheel 2 had the noisiest results as shown by its high RSD. In fact, the wheels on the right side of the rover had noisier values compared to the left side. The current drawn noise appears to have a greater influence than the wheel weight noise. This sensor noise could be attributed to noisier sensors or due to mechanically induced vibrations on the right side of the rover during its traverse.

The shearing resistance angle estimates have a downward bias. The output of the MLP will converge towards one of the training set values. In this case, the training set values for shearing angle are 30.3°, 30°, 25.7°, and

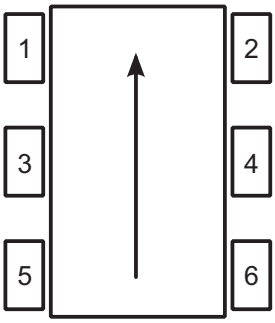

Fig. 5. Wheel numbering for rover showing forward direction of motion.

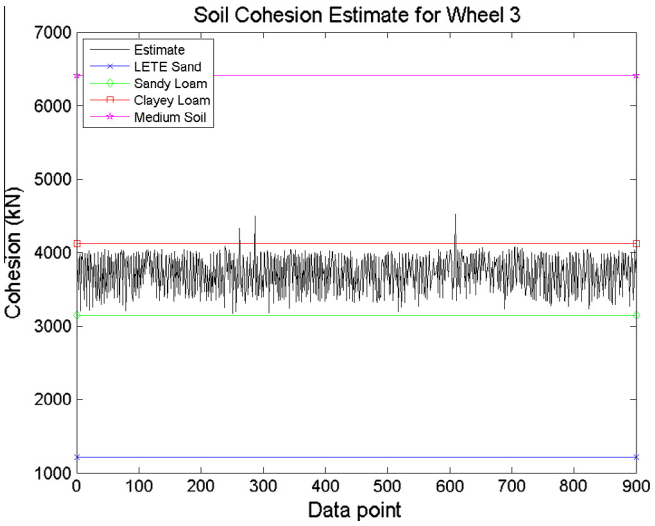

Fig. 6. Terrain cohesion estimate for Wheel 3 on prepared terrain.

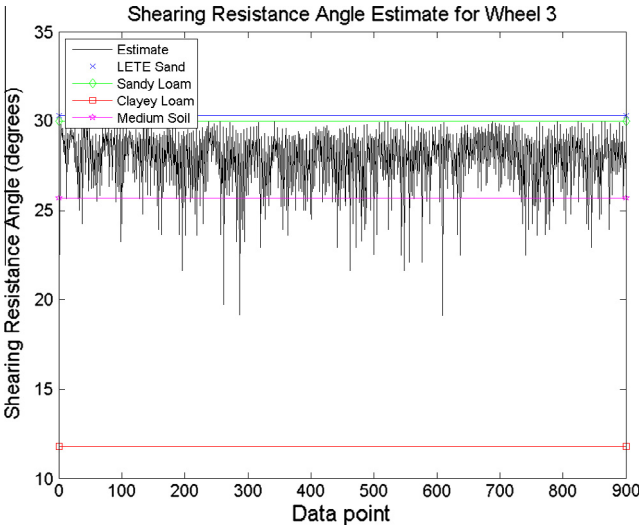

Fig. 7. Terrain shearing resistance angle estimate for Wheel 3 on prepared terrain.

11.8°. Most of the estimate points are between 25.7° and 30.3°. The remaining points converge towards the fourth value at 11.8°. Therefore, the results that do not converge

Table 3
Terrain parameter estimates for prepared terrain.

Wheel	Mean, c (Pa)	%RSD	Mean, ϕ (°)	%RSD
1	3832	7.6	27.5	8.4
2	3849	13.1	26.6	13.2
3	3726	6.4	27.8	6.5
4	3644	7.8.	26.5	9.4
5	3641	6.7	27.7	6.9
6	3737	11.5	26.2	11.4

Table 4
Relative standard deviation (RSD) for sensor data collected on prepared terrain.

Wheel	%RSD of I	%RSD of W
1	31.2	14.2
2	38.8	11.9
3	31.3	9.6
4	36.5	7.0
5	31.2	6.7
6	35.1	7.2

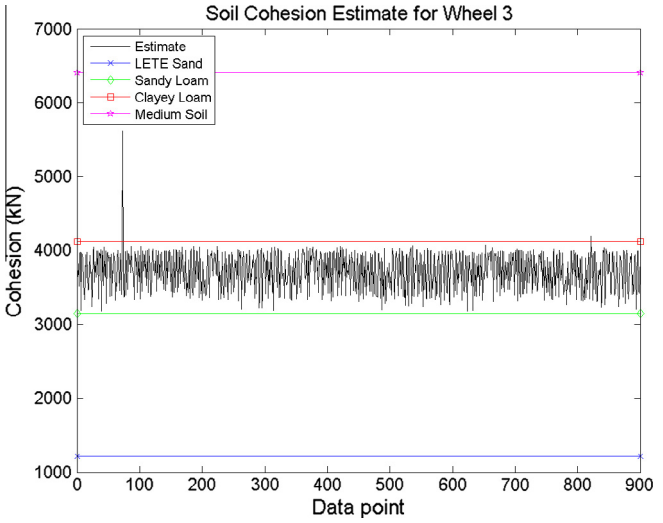

Fig. 8. Terrain cohesion estimate from Wheel 3 on unprepared terrain.

towards 25.7° or 30.3° will converge towards 11.8° as shown by the figures. This downward bias can be explained by the noisy current data when the current values are low. Lower current values translate into less torque required, which can be interpreted as the more cohesive training value (clayey loam) that has the shearing resistance angle of 11.8°.

The objective of estimating the terrain parameters is to detect when the cohesion or shearing angle decrease. A decrease in either one of these terrain parameters will result in a decrease in shear stress developed at the wheel-terrain interface. The consequence of decreased shear stress is the decrease in the maximum thrust developed by the rover wheels. When the developed thrust is insufficient to overcome terrain resistance, as was the case with *Spirit*, the rover will become immobilized.

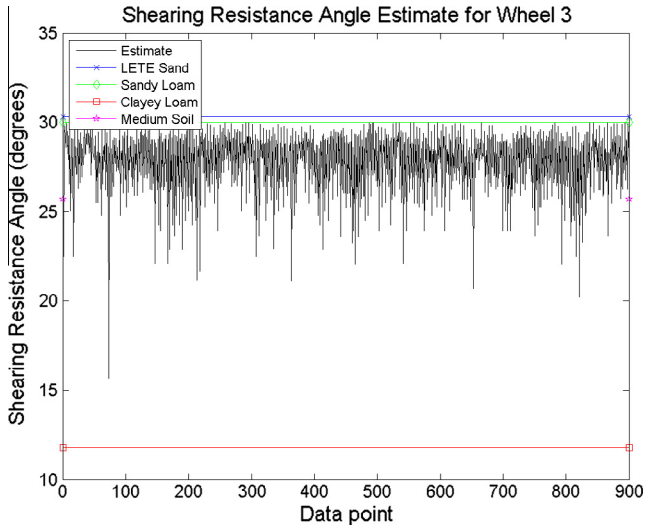

Fig. 9. Terrain shearing resistance angle estimate from Wheel 3 on unprepared terrain.

Table 5
Terrain parameter estimates for unprepared terrain.

Wheel	Mean, c (Pa)	%RSD	Mean, ϕ (°)	%RSD
1	3861	10.0	27.0	10.4
2	3931	17.5	25.8	16.3
3	3722	6.7	27.8	6.5
4	3693	9.4	26.3	10.3
5	3632	6.1	27.7	6.2
6	3711	7.6	27.2	7.7

Table 6
Relative standard deviation (RSD) for sensor data collected on unprepared terrain.

Wheel	%RSD of I	%RSD of W
1	33.4	16.1
2	42.4	14.7
3	31.6	9.3
4	36.1	9.4
5	30.7	6.6
6	29.2	7.2

4. Conclusions and future work

This paper identified a novel method for online terrain parameter estimation that does not require knowledge of the wheel sinkage depth. The preliminary results from terrestrial tests are a proof-of-concept that a trained neural network can provide an estimate of the terrain cohesion and internal shearing resistance online during the rover's traverse. Following conversations with engineers at NASA's Jet Propulsion Lab, there is hope to test this method of parameter estimation using data collected from the still mobile MER *Opportunity*. The target of this method has been Mars regolith however future simulations will apply this method to lunar regolith.

It is hoped that continuing to apply neural computing techniques to terramechanics theory will allow for more robust parameter estimation. Future work will require means of damping the erroneous values that arise from sensor noise without defeating the intent of detecting actual changes in the terrain parameters. The current MLP uses three sensors as inputs. Additional sensor data, such as vibrations from an IMU, could also serve as inputs so long as there is a model on how different terrain produces those data. Similarly, the effect of elevation will need to be incorporated. The tests presented in this paper occurred on level terrain and the neural network does not take elevation into account.

Acknowledgements

The authors thank the SEEG members (Chris Nicol, Tim Setterfield, Marc Gallant, Rob Hewitt, Brian Lynch, Adam Mack, Jesse Heimstra, Adam Brierly and Cameron Frazier) for their tireless contributions to the development and testing of the *Kapvik* instrumented chassis and mobility system; without their hard work and dedication research performed for this paper would not be possible. *Kapvik* was funded by the Exploration Surface Mobility (ESM) project of the Canadian Space Agency (CSA) and administered by MPB Communications Inc. Ryerson University, the University of Toronto Institute for Aerospace Studies, MacDonanld Detwiller and Associates, and Xiphos Technologies Inc. contributed to *Kapvik*'s development. The authors would also like to thank the reviewers for their thorough feedback during the review process to get this paper published.

References

[1] Arvidson RE, Bell JF, Bellutta P, Cabrol NA, Catalano JG, Cohen J, et al. Spirit Mars rover mission: overview and selected results from the northern home plate winter haven to the side of scamander crater. J Geophys Res 2010;115. http://dx.doi.org/10.1029/2010JE003633.
[2] Squyres SW, Arvidson RE, Bollen D, Bell JF, Brückner J, Cabrol NA, et al. Overview of the opportunity Mars exploration rover mission to meridiani planum: eagle crater to purgatory ripple. J Geophys Res 2006;111(E12). http://dx.doi.org/10.1029/2006JE002771.
[3] Shirley D, Matijevic J. Mars pathfinder microrover. Autonom Robots 1995;2(4):283–9. http://dx.doi.org/10.1007/BF00710795.
[4] Muirhead B. Mars rovers, past and future. In: 2004 IEEE aerospace conference proceedings (IEEE Cat. No.04TH8720). IEEE; 2004. p. 128–34. ISBN: 0-7803-8155-6, doi:10.1109/AERO.2004.1367598.
[5] Rivellini TP. Mars rover mechanisms designed for Rocky 4. In: The 27th aerospace mechanisms symposium; 1993.
[6] Chottiner J. Simulation of a six wheel martian rover called the rocker bogie. MSc thesis, The Ohio State University; 1992.
[7] Bekker M. Introduction to terrain-vehicle systems. University of Michigan Press; 1969.
[8] Wong JY. Terramechanics and off-road vehicle engineering. 2nd ed. Elsevier; 2010. ISBN: 9780750685610, doi:10.1016/B978-0-7506-8561-0.00014-2.
[9] Costes NC, Farmer JE, Marshall GC, Flight S. Mobility performance of the lunar roving vehicle: terrestrial studies-apollo 15 results. Apollo The International Magazine Of Art And Antiques; December 1972.

[10] Asnani V, Delap D, Creager C. The development of wheels for the lunar roving vehicle. J Terramech 2009;46(3):89–103. http://dx.doi.org/10.1016/j.jterra.2009.02.005.
[11] Shibly H, Iagnemma K, Dubowsky S. An equivalent soil mechanics formulation for rigid wheels in deformable terrain, with application to planetary exploration rovers. J Terramech 2005;42(1):1–13. http://dx.doi.org/10.1016/j.jterra.2004.05.002.
[12] Iagnemma K, Shibly H, Dubowsky S. On-line terrain parameter estimation for planetary rovers. Proceedings 2002 IEEE international conference on robotics and automation (Cat. No.02CH37292), vol. 3. IEEE; 2002. p. 3142–7. ISBN: 0-7803-7272-7, doi:10.1109/ROBOT.2002.1013710.
[13] Iagnemma K, Dubowsky S. Mobile robots in rough terrain: estimation, motion planning, and control with application to planetary rovers, star ed., vol. 12. Springer; 2004. ISBN: 3-540-21968-4.
[14] Yoshida K, Watanabe T, Mizuno N, Ishigami G. Slip, traction control, and navigation of a lunar rover. In: Proceedings of the 7th international symposium on artificial intelligence, robotics and automation in space; 2003.
[15] Ishigami G, Miwa A, Nagatani K, Yoshida K. Terramechanics-based model for steering maneuver of planetary exploration rovers on loose soil. J Field Robot 2007;24(3):233–50. http://dx.doi.org/10.1002/rob.20187.
[16] Bauer R, Leung W, Barfoot T. Experimental and simulation results of wheel–soil interaction for planetary rovers. In: 2005 IEEE/RSJ international conference on intelligent robots and systems. IEEE; 2005. p. 586–91. ISBN: 0-7803-8912-3, doi:10.1109/IROS.2005.1545179.
[17] Irani R, Bauer R, Warkentin a. A dynamic terramechanic model for small lightweight vehicles with rigid wheels and grousers operating in sandy soil. J Terramech 2011;48(4):307–18. http://dx.doi.org/10.1016/j.jterra.2011.05.001.
[18] Patel N, Slade R, Clemmet J. The ExoMars rover locomotion subsystem. J Terramech 2010;47(4):227–42. http://dx.doi.org/10.1016/j.jterra.2010.02.004.
[19] Kromer O. Adaptive flexible wheels for planetary exploration. In: 62nd International astronautical congress, Cape Town; 2011.
[20] Kleiner A. Online learning terrain classification for adaptive velocity control. In: 2010 IEEE safety security and rescue robotics. IEEE; 2010. p. 1–7. ISBN: 978-1-4244-8898-8, doi:10.1109/SSRR.2010.5981563.
[21] Brooks C, Iagnemma K. Vibration-based terrain classification for planetary exploration rovers. IEEE Trans Robot 2005;21(6):1185–91. http://dx.doi.org/10.1109/TRO.2005.855994.
[22] Brooks CA, Iagnemma KD. Self-supervised classification for planetary rover terrain sensing. In: 2007 IEEE aerospace conference. IEEE; 2007. p. 1–9. ISBN: 1-4244-0524-6, doi:10.1109/AERO.2007.352693.
[23] Tan C, Zweiri Y, Althoefer K, Seneviratne L. Online soil parameter estimation scheme based on NewtonRaphson method for autonomous excavation. IEEE/ASME Trans Mechatron 2005;10(2):221–9. http://dx.doi.org/10.1109/TMECH.2005.844706.
[24] Yousefi Moghaddam R, Kotchon A, Lipsett M. Method and apparatus for on-line estimation of soil parameters during excavation. J Terramech 2012;49(3–4):173–81. http://dx.doi.org/10.1016/j.jterra.2012.05.002.
[25] Wilcox BH. Non-geometric hazard detection for a Mars microrover. Tech. rep., Jet Propulsion Laboratory, Houston, Texas, USA; 1994.
[26] Reina G, Ojeda L, Milella A, Borenstein J. Wheel slippage and sinkage detection for planetary rovers. IEEE/ASME Trans Mechatron 2006;11(2):185–95. http://dx.doi.org/10.1109/TMECH.2006.871095.
[27] Hornik K, Stinchcombe M, White H. Multilayer feedforward networks are universal approximators. Neural Netw 1989;2(5):359–66. http://dx.doi.org/10.1016/0893-6080(89)90020-8.
[28] Ham FM, Kostanic I. Principles of neurocomputer for science and engineering. McGraw-Hill; 2001. ISBN: 0070259666.
[29] Haykin S. Neural networks: a comprehensive foundation. second ed. Prentice-Hall; 1999. ISBN: 0132733501.
[30] Ruck D, Rogers S, Kabrisky M, Maybeck P, Oxley M. Comparative analysis of backpropagation and the extended Kalman filter for training multilayer perceptrons. IEEE Trans Pattern Anal Mach Intell 1992;14(6):686–91. http://dx.doi.org/10.1109/34.141559.
[31] Georgios L. Neural networks and multimedia datasets: estimating the size of neural networks for achieving high classification accuracy. In: Proceedings of the 9th WSEAS international conference on Multimedia systems & signal processing; 2009. p. 237–42.
[32] Bartlett P. The sample complexity of pattern classification with neural networks: the size of the weights is more important than the size of the network. IEEE Trans Inform Theory 1998;44(2):525–36. http://dx.doi.org/10.1109/18.661502.
[33] Nguyen D, Widrow B. Improving the learning speed of 2-layer neural networks by choosing initial values of the adaptive weights. Int Joint Conf Neural Netw 1990;3:21–6. http://dx.doi.org/10.1109/IJCNN.1990.137819.
[34] Lyasko M. Slip sinkage effect in soilvehicle mechanics. J Terramech 2010;47(1):21–31. http://dx.doi.org/10.1016/j.jterra.2009.08.005.
[35] Charrett TOH, Waugh L, Tatam RP. Speckle velocimetry for high accuracy odometry for a Mars exploration rover. Measur Sci Technol 2010;21(2):025301. http://dx.doi.org/10.1088/0957-0233/21/2/025301.
[36] Okello A. A review of soil strength measurement techniques for prediction of terrain vehicle performance. J Agr Eng Res 1991;50:129–55. http://dx.doi.org/10.1016/S0021-8634(05)80010-1.